Journal of Physics: Conference Series **1586** (2020) 012027 doi:10.1088/1742-6596/1586/1/012027

Tests of the electroweak sector with precision measurements and diboson final states at the ATLAS Experiment.

L Fabbri

Università di Bologna and INFN.

E-mail: laura.fabbri@cern.ch

Abstract. The electroweak sector of the Standard Model can be tested either via precision measurements of fundamental observables or via direct tests of its underlying gauge structure. The ATLAS collaboration has recently released a measurement of the effective leptonic weak mixing angle using data collected at a centre-of-mass energy of 8 TeV. The result has a precision similar to that of the most precise individual measurements. The high integrated luminosity delivered by the LHC during Run-2 has allowed ATLAS to measure integrated and differential cross-sections for several kinematic observable of $W^{\pm}Z$ production in pp collisions and to observe vector boson scattering processes with WZ and same-sign WW final states. The results from these milestone analyses as well as their interpretation in the context of the Standard Model are presented in this proceeding.

1. Introduction

The Standard Model (SM) of particle physics provides a successful description of the fundamental particles and their interactions. Self-consistency of the SM can be tested by performing precision measurements of its parameters and confronting the results with theoretical predictions.

The study of $W^{\pm}Z$ or $W^{\pm}W^{\pm}$ diboson production is an important test of the SM for its sensitivity to gauge boson self-interactions which is related to the non-Abelian structure of the electroweak interaction. In particular, the scattering of two massive vector bosons (VBS) is a key process to probe the $SU(2)_L \times U(1)_Y$ gauge symmetry of the electroweak (EW) theory that determines the self-couplings of the vector bosons. In fact, new phenomena beyond the Standard Model can alter the couplings of vector bosons, generating additional contributions with respect to the predictions [1, 2, 3]. Improved constraints from precise measurements can potentially probe scales of new physics in the multi-TeV range and provide a way to look for signals of new physics in a model-independent way.

The production of $W^{\pm}Z$ or $W^{\pm}W^{\pm}$ provides the means to directly probe the triple gauge boson couplings (TGC), in particular the WWZ gauge coupling, and the quartic gauge couplings (QGC). Differential cross-section measurement of the scattering of vector bosons (VBS) $VV \to VV$ with $V = W/Z/\gamma$ can be used to test for an anomalous behaviour of the couplings.

In proton-proton (pp) collisions VBS processes produce final states with two gauge bosons and two jets ($VVjj$) via two classes of production mechanisms. The first class involves exclusively

weak interactions at Born level and is referred to as "*EW interaction*". The second class involves both strong and EW interactions at Born level and is referred to as "*strong production*". It includes both the EW gauge bosons via trilinear and quartic gauge interactions, and the EW non-VBS production where the two gauge bosons do not directly scatter. According to the SM a small interference occurs between production of EW and strong quark scattering. Compare to other VBS processes, the $W^{\pm}W^{\pm}jj$ channel has the largest ratio of EW to strong production cross-sections and tree-level diagrams not involving self interactions are suppressed [9].

This proceeding reports on the observation and measurement of EW production of the $W^{\pm}Zjj$ and $W^{\pm}W^{\pm}jj$ processes where vector bosons decay leptonically to electrons or muons.

The electroweak mixing angle, $\sin^2\theta^{\ell}_{\text{eff}}$, is connected at tree level with the W and Z boson masses, hence any inconsistency between these three measurements can give a hint for new physics. Nowadays, the global fit of the electroweak sector of the Standard Model indirectly constrains $\sin^2\theta^{\ell}_{\text{eff}}$ to 0.23149 ± 0.00007 [14, 15].

The ATLAS collaboration performed a measurement of the effective leptonic weak mixing angle, $\sin^2\theta^{\ell}_{\text{eff}}$, with an uncertainty comparable to the Tevatron final result [10] and lower than the most precise measurement at the LHC, recently published by the CMS collaboration [11]. Although not as accurate as the lepton collider legacy result [12, 13], the hadron-collider measurements improve the overall consistency of the full set of measurements of $\sin^2\theta^{\ell}_{\text{eff}}$.

The result is obtained extending the analysis devoted to the measurement of the angular coefficients describing Z boson events [16].

2. Precision WZ and WW measurements at 13 TeV

2.1. Event selections.

The presented results are obtained using pp collisions recorded by the ATLAS detector [4] at the center-of-mass energy of $\sqrt{s} = 13$ TeV in 2015 and 2016, corresponding to an integrated luminosity of 36.1 fb^{-1}. The W and Z bosons are reconstructed using their decay modes into muons or electrons. Total and single differential cross-sections as function of various kinematic variables, including a measure of jet activity in $W^{\pm}Z$ events, are performed and compared with the SM predictions at the next-to-leading order (NLO) in QCD [5, 6] and with the recent calculations at next-to-next-to-leading order (NNLO) [7].

VBS $VVjj$ production has a very peculiar kinematical signature: it produces two high p_{T} forward jets and two vector bosons produced in the central region. The complete selection criteria are reported in Ref. [17, 18] for the WZ and in Ref. [19] for the same-sign W boson pair production.

All final states with three charged leptons (electrons e or muons μ) and $E_{\text{T}}^{\text{miss}}$ from $W^{\pm}Z$ leptonic decays are considered and are classified in four categories according to the different final states. They are referred to as $\mu^{\pm}\mu^{+}\mu^{-}$, $e^{\pm}\mu^{+}\mu^{-}$, $\mu^{\pm}e^{+}e^{-}$ and $e^{\pm}e^{+}e^{-}$, where the first label is from the charged lepton of the W decay, and the last two labels are for the Z decay. No requirement on the number of jets is applied.

Concerning the $W^{\pm}W^{\pm}$ production, only W decays to $e\nu_e$ and $\mu\nu_\mu$ are considered. They consist of two same-sign charged leptons (electrons e or muons μ) and $E_{\text{T}}^{\text{miss}}$ and classified in three categories according to the different final states, referred to as $e^{\pm}e^{\pm}$, $e^{\pm}\mu^{\pm}$ and $\mu^{\pm}\mu^{\pm}$.

2.2. WZ Cross-section measurements.

For a given channel $W^{\pm}Z \to \ell'^{\pm}\nu\ell^{+}\ell^{-}$, where ℓ and ℓ' refer to either an electron or a muon, the integrated fiducial cross-section that includes the leptonic branching fractions of the W and Z bosons is calculated by means of the measured number of observed events and the estimated number of background events in a standard way [17]. The measured fiducial cross-sections in

the four channels are combined using a χ^2 minimisation method that accounts for correlations between the sources of systematic uncertainty affecting each channel. The result is a weighted mean value corresponding to the cross-section of $W^{\pm}Z$ production and decay to a single leptonic channel, with muons or electrons, in the fiducial phase space. In Figure 1 the measured cross-sections are compared with the corresponding SM NNLO QCD prediction from MATRIX [7] using both the NNPDF3.0nnlo and the MMHT PDF sets and the NLO prediction from Sherpa 2.2.2 [8].

For the measurements of the differential distributions, all four decay channels, $\mu^{\pm}\mu^{+}\mu^{-}$,$e^{\pm}\mu^{+}\mu^{-}$, $\mu^{\pm}e^{+}e^{-}$ and $e^{\pm}e^{+}e^{-}$, are added together. The resulting distributions are unfolded with a response matrix computed using a Powheg+Pythia MC signal sample that includes all four topologies such that cross-sections refer to final states where the W and Z decay in a single leptonic channel with muons or electrons.

The $W^{\pm}Z$ production cross-section is measured as a function of several variables: the transverse momentum of the Z and W boson, $p_{\mathrm{T}}^{\mathrm{Z}}$ and $p_{\mathrm{T}}^{\mathrm{W}}$, the transverse mass of the $W^{\pm}Z$ system, $m_{\mathrm{T}}^{\mathrm{WZ}}$, the azimuthal angle between the W and Z bosons, $\Delta\phi(W,Z)$, the p_{T} of the neutrino associated with the decay of the W boson, p_{T}^{ν}, the absolute difference between the rapidities of the Z boson and the charged lepton from the decay of the W boson, $|y_{\mathrm{Z}} - y_{\mathrm{l,W}}|$, the exclusive jet multiplicity, N_{jets}, and the invariant mass of the two leading jets,m_{jj}. The measured differential cross-sections are compared to the predictions at NNLO in QCD from the MATRIX computational framework corrected from Born-level leptons to dressed leptons, to NLO MC predictions from Powheg+Pythia, after a rescaling of its predicted integrated fiducial cross-section to the NNLO cross-section, and to Sherpa 2.2.2. A good description of the measured cross-sections is observed. The distributions in $p_{\mathrm{T}}^{\mathrm{Z}}$ and $m_{\mathrm{T}}^{\mathrm{WZ}}$ are especially interesting because are sensitive to anomalous TGC: no excess of data is observed (Fig. 2).

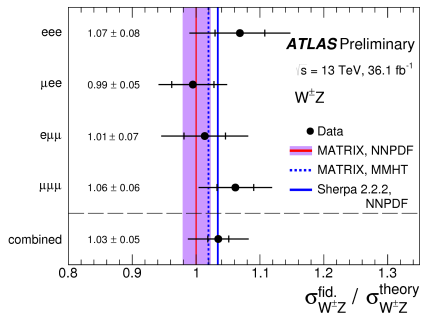

Figure 1. Ratio of the measured $W^{\pm}Z$ integrated cross-sections in the fiducial phase space to the theoretical predictions as described in the text. For more details see Ref. [17].

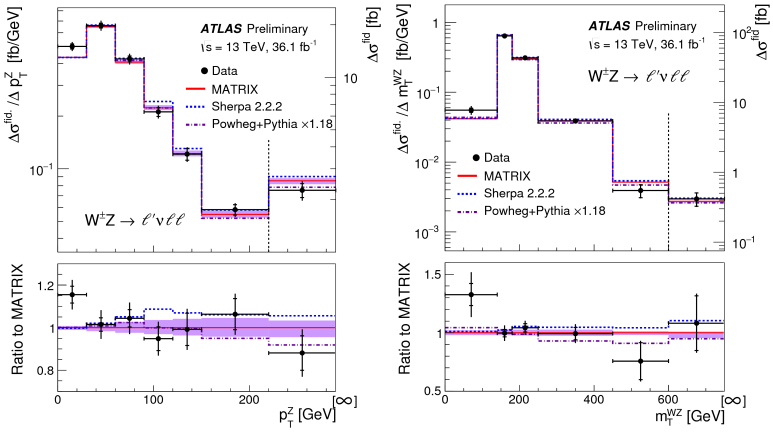

Figure 2. The measured $W^{\pm}Z$ differential cross-section in the fiducial phase space as a function of $p_{\mathrm{T}}^{\mathrm{Z}}$ (left) and $m_{\mathrm{T}}^{\mathrm{WZ}}$ (right). The measurements are compared to the theoretical calculations. For details see text and Ref. [17].

2.3. $W^{\pm}W^{\pm}jj$ EW production cross-section.

The $W^{\pm}W^{\pm}jj$ EW production and its interference with the $W^{\pm}W^{\pm}jj$ strong production cross-section is measured by means of a likelihood function. The signal region is defined as $m_{\mathrm{jj}} > 500$ GeV, where the m_{jj} distribution is split into four bins optimised to increase the signal

sensitivity. Thirty bins of the m_{jj} distributions of the signal and control regions are combined in a profile likelihood fit to extract the $W^{\pm}W^{\pm}jj$ EW production cross-section. The likelihood function is a product of Poisson probability density functions where each term is a function of the predicted signal and background event yields in one bin. The sources of systematic uncertainty are included in the fit as nuisance parameters constrained by a Gaussian function.

An excess of data events over the background predictions is observed in most of the bins. A total of 122 candidate events is observed for a background expectation of 78 ± 15 events before the fit. The total number of predicted background events after the fit is 69 ± 10. The observed excess of data events is consistent with the expected signal from $W^{\pm}W^{\pm}jj$ EW production. The background-only hypothesis is rejected with a significance of 6.9σ where a significance of 4.6σ is expected for the signal predicted by Sherpa. The measured fiducial cross-section is $\sigma^{\text{fid}} = 2.91^{+0.51}_{-0.47}(\text{stat.}) \pm 0.27(\text{sys.})$ fb, compared to $2.01^{+0.33}_{-0.23}(\text{sys.+stat.})$ fb predicted by Sherpa. The measured fiducial cross-section agrees with the prediction by Powheg+Pythia of $3.08^{+0.45}_{-0.46}$ (sys.+stat.) fb. The results are shown in Figure 3. The theoretical predictions include neither the interference of $W^{\pm}W^{\pm}jj$ EW and strong production, nor the NLO EW corrections, while the observed cross-section includes the $W^{\pm}W^{\pm}jj$ EW production and interference effects.

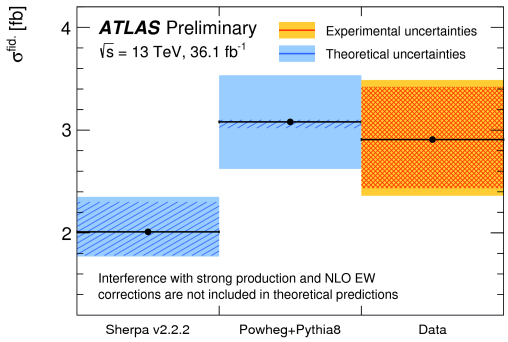

Figure 3. Comparison of the measured fiducial cross-section and the theoretical calculations as described in the text. For more details see Ref. [19].

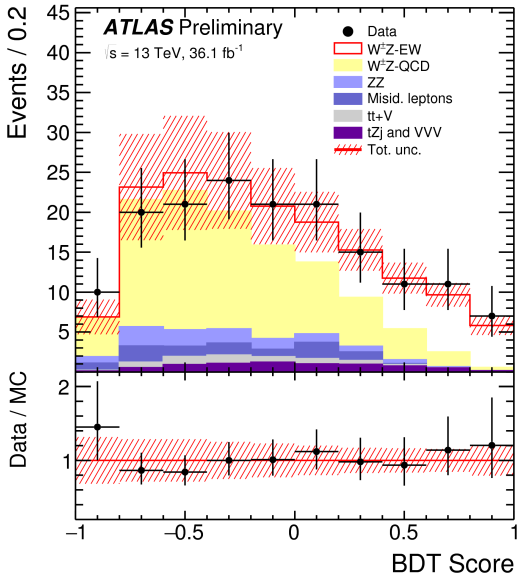

Figure 4. Post-fit BDT score distributions in the signal region. Signal and backgrounds are normalised to the expected number of events after the fit [18].

2.4. $W^{\pm}Zjj$ EW production cross-section.

The $W^{\pm}Zjj$ EW production cross-section is also measured by means of a likelihood function. Given the low purity in $W^{\pm}Zjj$ EW processes in the signal region, which is dominated by $W^{\pm}Zjj$ strong processes, a multivariate discriminant is therefore used to separate the signal and the backgrounds. A boosted decision tree (BDT), as implemented in the TMVA package [20] is used to exploit the kinematic differences between the $WZjj$-EW signal and the $WZjj$-strong and other backgrounds. It is trained and optimised on simulated events to separate signal events from all other background processes. A total of 15 variables are combined into one

discriminant. The distribution of the BDT score in the $W^{\pm}Zjj$ signal region (Fig. 4) is used to extract the significance of the $W^{\pm}Zjj$ -EW signal and to measure its fiducial cross-section via a maximum-likelihood fit. The background-only hypothesis is excluded in data with a significance of 5.6 standard deviations, for 3.3 standard deviations expected. The determination of the fiducial cross-section is carried out using the signal strength parameter μ_{EW}:

$$\mu_{EW} = \frac{N_{\text{data}}^{\text{signal}}}{N_{\text{MC}}^{\text{signal}}} = \frac{\sigma_{\text{meas.}}^{\text{fid. EW}}}{\sigma_{\text{MC}}^{\text{fid. EW th.}}} \tag{1}$$

where $N_{\text{i}}^{\text{signal}}$ are the signal yields in the data and predicted by the Sherpa MC simulation. The measured cross-section $\sigma_{\text{meas.}}^{\text{fid., EW}}$ is derived from the signal strength μ_{EW} by multiplying it by the Sherpa MC cross-section prediction $\sigma_{\text{MC}}^{\text{fid., EW th.}}$ in the fiducial region. The result is

$$\sigma_{\text{meas.}}^{\text{fid. EW}} = 0.57^{+0.15}_{-0.14}(\text{stat.})^{+0.05}_{-0.04}(\text{syst.})^{+0.04}_{-0.03}(\text{th.})\text{fb}. \tag{2}$$

The MC $WZjj$-strong contribution which is subtracted from data in the fit procedure does not contain interferences between the strong and EW processes. The measured cross-section $\sigma_{\text{meas.}}^{\text{fid. EW}}$ therefore formally corresponds to the cross-section of the EW production including interference effects. It is found to be larger than the LO SM prediction of 0.32 ± 0.03 fb as calculated with the Sherpa MC event generator which includes neither interference effects nor NLO EW corrections. Such calculation of higher order EW effects does not exist yet for the $W^{\pm}Zjj$ final state.

3. Measurement of the effective leptonic weak mixing angle

At leading order in EW theory, the full five-dimensional differential cross-section describing the kinematics of the two Born-level leptons from the Z boson decay can be decomposed as the unpolarised cross-section ($\sigma^{\text{U+L}}$), which factorises a sum of nine harmonic polynomials dependent on $\cos\theta$ and ϕ (in the Collins-Soper (CS) reference frame [21]), multiplied by eight dimensionless angular coefficients $A_{0\text{-}7}(p_{\text{T}}^{\ell\ell}, y^{\ell\ell}, m^{\ell\ell})$. At lowest order (LO) in QCD, only the annihilation diagram $q\bar{q} \to Z$ is present and only one coefficient (A_4) is non-zero, reducing the representation to a simpler three-dimensional differential cross-section:

$$\frac{d\sigma}{dy^{\ell\ell}dm^{\ell\ell}d\cos\theta} = \frac{3}{16\pi}\frac{d\sigma^{\text{U+L}}}{dy^{\ell\ell}dm^{\ell\ell}}\Big\{(1+\cos^2\theta) + A_4\cos\theta\Big\} \tag{3}$$

The angular coefficients are extracted from the data by fitting templates of the P_i polynomial terms to the reconstructed angular distributions using 8×8 bins in $(\cos\theta, \phi)$ space (as described in detail in Ref. [16]). A likelihood fit is built taking into account a long list of uncertainties as completely described in Ref. [22]. This analysis focuses on the A_4 angular coefficient determination, which is the most sensitive to $\sin^2\theta_{\text{eff}}^{\ell}$. The full data sample, collected in 2012 at $\sqrt{s} = 8$ TeV at the LHC and corresponding to an integrated luminosity of 20.2 fb^{-1}, is split into three orthogonal channels that are analysed independently, and then combined for the last stages of the analysis. These channels are: two electrons in the central region ($ee_{\text{CC}}, \sim 6M$ events), two muons in the central region ($\mu\mu_{\text{CC}}, \sim 7.5M$ events) and one central and one forward electron ($ee_{\text{CF}}, \sim 1.5M$ events). The results for $\sin^2\theta_{\text{eff}}^{\ell}$ are obtained individually per analysis channel, as well as for the combination of the central-central channels and for the full combination, which includes the central- forward channel that has the highest sensitivity. The combined result is measured to be:

$$\sin^2\theta_{\text{eff}}^{\ell} = 0.23140 \pm 0.00021(\text{stat.}) \pm 0.00024(\text{PDF}) \pm 0.00016(\text{syst.}) \tag{4}$$

where the first uncertainty corresponds to the data statistical uncertainty, the second to the PDF uncertainties in the MMHT14 PDF set, and the third to all other systematic uncertainties affecting the measurement and its interpretation. This result agrees within its total uncertainty of ± 0.00036 with the current value of 0.23150 ± 0.00006 from global electroweak fits [14].

4. Conclusions

Precise measurements of SM quantities are performed both at $\sqrt{s} = 8$ and 13 TeV center-of-mass energy by the ATLAS Collaboration. Integrated and differential cross-section of $W^{\pm}Z$ at 13 TeV are measured and compared with theoretical expectations. The first observations of $W^{\pm}W^{\pm}jj$ and $W^{\pm}Zjj$ production via VBS are reported. A precise polarisation study of the Z boson at 8 TeV leads to the best measurement at LHC of $\sin^2\theta^{\ell}_{\text{eff}}$, which is found to be in agreement with the current value obtained from global electroweak fits.

References

[1] O. J. P. Eboli, M. C. Gonzalez-Garcia and S. M. Lietti, Bosonic quartic couplings at CERN LHC, *Phys. Rev. D* **69** (2004) 095005.
[2] C. Degrande et al., Effective Field Theory: A Modern Approach to Anomalous Couplings, *Annals Phys.* **335** (2013) 21.
[3] D. Espriu and B. Yencho, Longitudinal WW scattering in light of the "Higgs boson" discovery, *Phys. Rev. D* **87** (2013) 055017.
[4] ATLAS Collaboration, The ATLAS Experiment at the CERN Large Hadron Collider, *JINST* **3** (2008) S08003.
[5] J. Ohnemus, Order-α_s calculation of hadronic $W^{\pm}Z$ production, *Phys. Rev. D* **44** (1991) 3477.
[6] S. Frixione, P. Nason and G. Ridolfi, Strong corrections to WZ production at hadron colliders, *Nucl. Phys. B* **383** (1992) 3.
[7] M. Grazzini, S. Kallweit, D. Rathlev and M. Wiesemann, $W^{\pm}Z$ production at the LHC: fiducial cross-sectiontions and distributions in NNLO QCD, *JHEP* **1705** (2017) 139.
[8] T. Gleisberg et al., Event generation with SHERPA 1.1, *JHEP* **0902** (2009) 007.
[9] M. Szleper, The Higgs boson and the physics of WW scattering before and after Higgs discovery, (2014)., arXiv: 1412.8367 [hep-ph].
[10] CDF and D0 Collaborations, Tevatron Run II combination of the effective leptonic electroweak mixing angle, *Phys. Rev. D* **97** (2018) 112007.
[11] CMS Collaboration, Measurement of the weak mixing angle using the forward-backward asymmetry of Drell-Yan events in pp collisions at 8 TeV, *Eur. Phys. J. C* **78** (2018) 701.
[12] ALEPH, DELPHI, L3, OPAL, and SLD Collaborations, LEP and SLD Electroweak Working Groups, Precision electroweak measurements on the Z resonance, *Phys. Rept.* **427** (2006) 257.
[13] ALEPH, DELPHI, L3, and OPAL Collaborations, LEP Electroweak Working Group, A Combination of preliminary electroweak measurements and constraints on the standard model, (2006).
[14] The GFITTER Group, The electroweak fit of the standard model after the discovery of a new boson at the LHC,Êur. Phys. J. C **72** (2012) 2205.
[15] The GFITTER Group, The global electroweak fit at NNLO and prospects for the LHC and ILC, *Eur. Phys. J. C* **74** (2014) 3046.
[16] ATLAS Collaboration, Measurement of the angular coefficients in Z-boson events using electron and muon pairs from data taken at $\sqrt{s} = 8$ TeV with the ATLAS detector, *JHEP* **08** (2016) 159.
[17] ATLAS Collaboration, Measurement of $W^{\pm}Z$ production cross-sections and gauge boson polarisation in pp collisions at $\sqrt{s} = 13$ TeV with the ATLAS detector. *Eur. Phys. J. C* **79** (2019) 535.
[18] ATLAS Collaboration, Observation of electroweak $W^{\pm}Z$ boson pair production in association with two jets in pp collisions at $\sqrt{s} = 13$ TeV with the ATLAS detector. *Phys. Lett. B* **793** (2019) 469.
[19] ATLAS Collaboration, Observation of electroweak production of a same-sign W boson pair in association with two jets in pp collisions at $\sqrt{s} = 13$ TeV with the ATLAS detector. ATLAS-CONF-2018-030, http://cdsweb.cern.ch/record/2629411
[20] A. Hoecker et al., TMVA: Toolkit for Multivariate Data Analysis, *PoS ACAT* (2007) 040.
[21] J. C. Collins, D. Soper and E. Davison, Angular distribution of dileptons in high-energy hadron collisions, *Phys. Rev. D* **16** (1977) 2219,
[22] ATLAS Collaboration, Measurement of the effective leptonic weak mixing angle using electron and muon pairs from Z-boson decay in the ATLAS experiment at $\sqrt{s} = 8$ TeV . ATL-CONF-2018-037, http://cdsweb.cern.ch/record/2630340